Nano World Journal

https://doi.org/10.17756/nwj.2023-s3-172

Research Article

Open Access

Revolutionizing Nanomaterial Defect Detection with Deep Learning Algorithms

Lenin Kathiresan[1], Luis Buenaño[2], Sayuri Bonilla[3], Freddy Ajila[3], Vanessa Valverde[4], Harshitha Kuntamukkula[5] and Mayakannan Selvaraju[6*]

[1]Research Scholar, Chennai Institute of Technology, Anna University, Chennai, India
[2]Department of Mechanical Engineering, Escuela Superior Politécnica de Chimborazo (ESPOCH), Riobamba, Ecuador
[3]Facultad de Informática y Electrónica, Escuela Superior Politécnica de Chimborazo (ESPOCH), Sede Orellana, El Coca, Ecuador
[4]Facultad de Mecánica, Escuela Superior Politécnica de Chimborazo (ESPOCH), Ecuador
[5]School of Architecture, Koneru Lakshmaiah Education Foundation, Vaddeswaram, Guntur District, Andhra Pradesh, India
[6]Department of Mechanical Engineering, Vidyaa Vikas College of Engineering and Technology, Tiruchengode, Namakkal, Tamil Nadu, India

***Correspondence to:**
Mayakannan Selvaraju
Department of Mechanical Engineering,
Vidyaa Vikas College of Engineering and Technology,
Tiruchengode, Namakkal, Tamil Nadu, India.
E-mail: kannanarchieves@gmail.com

Received: July 31, 2023
Accepted: November 01, 2023
Published: November 03, 2023

Citation: Kathiresan L, Buenaño L, Bonilla S, Ajila F, Valverde V, et al. 2023. Revolutionizing Nanomaterial Defect Detection with Deep Learning Algorithms. *NanoWorld J* 9(S3): S973-S979.

Published by United Scientific Group

Abstract

As nanotechnology progresses, scientists have more options than ever for processing nanomaterials. Recent advances in nanotechnology have led to widespread interest in using nanomaterials for detection and catalysis. Particularly impressive are the biocompatibility, plasma surface resonance absorption, and Raman surface enhancement features of metal nano molecules. In addition to being highly absorbent of plasma surface resonance and exhibiting increased Raman surface activity, metal nano molecules are also biocompatible. In this study, researchers investigate a defect detection and classification method for metallic nanomaterials that is based on deep learning (DL). By observing occurrences in the lab, we may learn about and improve methods for detecting flaws in metal nanoparticles, as well as assess challenges and plan for their manufacture. Research is conducted on the DL algorithm, the first mock-up model of a DL network, a multi-mode method for detecting metal faults, and a classification system for surface defects. Using DL, flaws in metal nanomaterials may now be identified. It is possible to identify metal flaws quantitatively and to see the whole defect. Single-mode, conventional, nondestructive testing equipment is unable to identify smaller defects. It's challenging due of the lack of reliable quantitative detection. The findings indicate that there are five distinguishing factors for identifying nano-surface defects in metals. The DL-based defect identification and sorting method can be useful in materials maintenance since it makes use of big data technology to assess the full dataset of problems, as well as data on the surrounding environment and the level of effort put in by workers. It's also crucial for progress in nano-detection technologies for metals.

Keywords

Nanomaterials, Defects, Detection, Algorithms, Classification

Introduction

Exploring the unique features that depend on morphology has received interest as the production of nanoparticles with controlled morphology has advanced steadily [1]. Due to their exceptional physical and chemical characteristics, metal nanoparticles are gaining attention as a potential tool for better catalysis and chemistry, metal nanoparticles, which are employed in many different surface-enhancement applications, have optical characteristics that vary depending on their size, shape, surface function, and structural composition [2]. Several instances of this phenomenon include Raman spectroscopy, fluorescence

enhancement, analysis, and sensing. These applications find utility in medical diagnostics and biological technology.

Researchers have recently begun exploring different ways to modify the size, structure, and chemical make-up of metal nanoparticles. The pursuit of exact optical characteristics and the promotion of catalytic chemical processes are the primary motivations for this study. Size, shape, and general structural qualities of metal nanoparticles are often intricately linked to their properties [3, 4]. These nanoparticles' properties are influenced by their structural attributes. Thus far, metals' nanoparticles have been successfully produced in a wide array of shapes and dimensions, ranging from zero-dimensional to one-dimensional and two-dimensional to three-dimensional structures [5]. Multicomponent noble metal nanocrystals have had their electrochemical characteristics altered due to their adaptability to modifications in both composition and form. Substantial advancements have been made in recent years towards precisely controlling the synthesis of intricate nanostructures composed of precious metal alloys [6]. Nano frames/nanostructures, nano trees/nanostructures, nano concave-convex structures, nano core-shell structures, etc., are all examples of these nanostructures. Metal nanoparticles of varying structures, as well as the bimetallic complexes that result from their union, are synthesized [7].

In the realm of nanotechnology, metal nano molecules have been the subject of the greatest research. Using DL, a fingerprint of the network's ownership value is developed. DL is a form of machine learning that achieves high levels of data abstraction by utilizing multi-layered neural networks (NN) composed of intricate structures and nonlinear transformations [8]. Complex NN have gained a lot of interest and been used in many different areas because of the rise of available data and the improvement of computational power. There is a paucity of concrete examples in this paper's summary of DL in NN, which covers a range of topics including common structural models and training techniques [9]. Authors [10] focus that recent advances in machine learning, particularly DL, are useful for spotting, categorizing, and quantifying patterns in medical images. Functions that are learnt from data alone, as opposed to knowledge-based functions constructed by hand, can be used to indicate Podstaw progress. Today, DL is the cutting edge of innovation [11]. Using DL, computers have successfully diagnosed and prognosed illnesses, and the way forward has been laid out [12]. However, the requisite experimental data is insufficient. The rising demand for indoor location-based services has led to the rise in popularity of fingerprint-based indoor positioning. This is because of the great precision with which it can pinpoint a person's precise location [13]. This motivates the proposal of a DL approach to fingerprint identification using channel state data. During both the offline training phase and the online positioning phase, the estimated location is determined through a probability-based method that relies on the principal radial function. There are three ways that may be utilized as a point of reference, however some of the talks are inaccurate [14].

This study contributes new knowledge by using a DL system to classify nanoscale metal surface defects, simulate a multimode metal defect detection approach, and conduct experimental research. Despite the advantages and disadvantages of currently used methods for detecting metal nanomaterials, there is much to gain economically and socially by exploring DL-based metal nano detection technologies.

Algorithm for DL

Network model of DL

Self-encoder network

There are three distinct BP network layers in total: the input, the hidden, and the output. The reconstruction layer is the output layer. If the error is tolerated, then the output will fully rebuild the input and both will be consistent. Both an encoder and a decoder make up the self-coder network. The larger the disparity between input and output, denoted by the error, the more efficient the network [15]. Let's call the encoding and decoding functions R and H, respectively.

$$g = r(x) = s(ax + b) \tag{1}$$

$$f = h(x) = y(cx + d) \tag{2}$$

$$f = (h - f + p)/a + 1 \tag{3}$$

Where

ax and cx = weightage of the matrix;

s = encoding activation functions;

y = decoding activation functions; and

b and d = offset terms.

Unsupervised learning is used by the self-repeated encoder's encoding and decoding to reduce error. When employed for image denoising, for instance, a cleaner image is obtained that is more amenable to further processing [16, 17]. Expansion constants such as these can be modified in practice by modifying the self-encoder and training process.

DL NN

Feature selection in conventional machine learning approaches is typically reliant on humanoid expert knowledge. This approach is ineffective, and it may even lead to incorrect feature selection when confronted with difficult recognition problems [18]. Automatically learning rich feature-related information, DL may be used to extract functions from a database in a layer-by-layer fashion [19]. Meanwhile, as demonstrated in figure 1, the DL network's nonlinear structure has great generalization capacity and can get quite close to the real-world complex-functions model.

Once linear input data is not available, a high-dimensional linear separation space should be utilized instead. Traditional machine learning deployments need significant investment of time and material. Since DL is a multilayer process, it can improve detection accuracy beyond that of standard machine learning by approximating nonlinear functions with a small number of parameters.

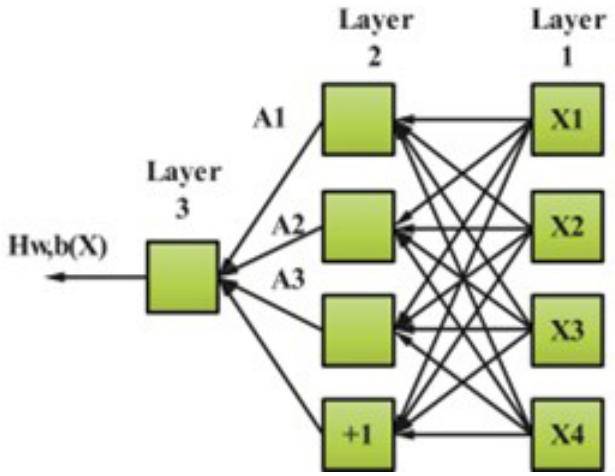

Figure 1: DLNN.

Metal nano detection using a temperature field equation

In photoacoustic non-destructive testing, the photoacoustic effect is typically induced through the thermoelastic mechanism and controlled by the laser energy density. This process involves the generation of an elastic stress field when a fraction of the laser energy (represented as G) is riveted and converted into heat as a pulsed laser beam is directed onto the material's surface. This results in a localized increase or decrease in temperature T and a corresponding increase or decrease in volume.

$$g = I_0 f(x, y, z)\, h(t)\, a \tag{4}$$

The pulsed laser's focal intensity; a = the material's absorption coefficient; f (x, y, z) = Laser power distribution in space, h = Obtain the equation for the linear elastic dynamic field. The strain equation is given in the following formula:

$$\nabla\sigma = \rho a \tag{5}$$

Photoacoustic reactions on metal nanoparticles produce a wide variety of ultrasonic waves. Ultrasonic wave modes generated by the photoacoustic effect can be more easily analyzed and theoretically model them as plane simple harmonic waves with amplitude vectors f (R, t) and phase velocities R, K, V on a uniform limitless elastic material [20, 21]:

$$f(r, t) = f \cdot \exp\,[ik(r - vt)] \tag{6}$$

$$h = kv = 2\pi v/\lambda \tag{7}$$

Where,

k = wave number;

h = angular frequency;

v = phase velocity; and

k = regularization coefficient.

$$f(x) = \sum_{n=1}^{M} h_n G(x, x_n) \tag{8}$$

Solving the problem of propagating a linear elastic dynamic field calls for a unique solution and careful judgment. To determine whether the eigenvalue of the Christoffel matrix, denoted as T, is a real integer, you should analyze the characteristic equation associated with it.

$$\det(T - \delta p v^2) = 0 \tag{9}$$

Detection of Defects in Nanoscale Metals and Related Experiments

Nano metal application

Free-flowing electrons and incoming electromagnetic radiation together oscillate to create plasma resonance at the surface of valuable metals. SPR peak absorption spectra of dissolved 20 nm Au NPs, for instance, are relatively intense. As Au NPs clump together, the shifting SPR peaks cause the solution to shift colors. A colour sensor based on this principle may be used to detect a wide range of analytes. This sensor type can detect analytes quickly, visually, and directly, saving time and money. Hupp invented the colorimetric sensor currently used for detecting heavy metals. Excitons of ionomers have been shown to boost electromagnetic radiation at the particle's surface in gold and silver nanoparticles in the 10 - 200 nm size range. Metal nanoparticles' SPR absorption may be tuned by manipulating their dimensions, surface chemistry, and surrounding medium. The high connection between the localized SPRS of the nanostructures also causes the SPR bands to shift dramatically when the nanoparticles are near one another. It is simple to control SPR absorption due to the many synthesized metal nanostructures of varying sizes, forms, and architectures. For color recognition by human eyes, nothing beats Au NPs among plasma nanoparticles. The human eye can readily discern the transition between red and blue, which has led to its widespread application.

Multimodal defect detection in metals: a modeling effort

There is a wide variety of shape, load, and material qualities to consider in the physical field. In most circumstances, there is no unique analytical solution to either the associated ordinary differential equation or the accompanying partial differential equation. For the eight generic phase approximations that may be used to derive the formula and solve the engineering issues, the finite element approach is required. Steps 1 and 8 (configuration and processing) are normally performed by humans, whereas steps 2 - 7 are handled by machines. Table 1 summarizes the stress-strain and stress-displacement correlations related with the various approaches of creating the simulated photoacoustic effect.

The metal impurity alumina in steel is chosen as an example. Positioned 15 - 24 mm above ground, with a 9 - 9.5 mm diameter target area. The excitation source simulation results shown in table 2 were obtained by switching the excitation location once every simulation and carrying out three simulations in total. Steel, alumina, and the combination of the two are all represented by one of the three activation points.

Seam defect quantification using pulsed eddy current techniques

Eddy current testing utilizes eddy currents to provide insights into a specimen. This is achieved by monitoring the superimposed signal that arises from the interaction between the primary and the secondary magnetic field. Through this

Table 1: Electrodynamic field equation with linear steps.

Step	Initialize and discretize the model
1	Choose the displacement function
2	An introduction of boundary conditions
3	Describe the displacement of stress and strain
4	Determining the number of degrees of freedom
5	Form the matrix and the equation for stiffness of elements are generated
6	Discuss the findings

Table 2: Finite element model steel material parameters.

Parameters	Value
Poisson's ratio	0.6
Specific heat capacity	500
Density	8000
Thermal conductivity	60
Modulus of elasticity	4
Thermal expansion coefficient	10^{-5}

process, we can effectively evaluate the presence of defects within the tested components. The strength of the secondary magnetic field (B) generated by the primary magnetic field (created by a spiral eddy current, I) on the conductive specimen is influenced by factors such as the defect's conductivity, the coil's position, and the coupling connection between the coil and the specimen. The generated current in pulsed eddy current testing decreases exponentially with depth due to the skin effect. Standard penetration depth, however, is determined otherwise. When conducting pulsed eddy current testing, a signal with a rectangular square wave shape and countless harmonic components of varying frequencies is used as the excitation.

Let this time be the square wave's excitation period, Δ be the pulse width [22, 23],

$$t = k\,\Delta$$

Incentives and boundary conditions

For a module that deals with low-frequency electromagnetic fields, the magnetically isolated boundary state is the default. According to the governing equation, the magnetic potential is zero at the interface.

The linkage between the state of a fracture defect and the nondestructive eddy current quarterly model is established through the concept of a magnetic isolation barrier. In this context, both the external current density and the region covered by the multi-turn coil can be employed for excitation purposes.

Using the rectangle as a stand-in for the coil's cross section and applying the external current density to it is one technique to estimate the current in a multi-turn coil, whose number of turns, current, and conductivity are all specified by the coil's domain. For more precise models and computations, multi-turn coil excitation application approach is preferable to external current density excitation. The efficiency of the detecting section is affected by the excitation coil's inner diameter, turn number, and height since it is responsible for loading the pulse signal. On the infinitely deep planar conductor, the eddy current density first increases and then decreases with increasing radial distance from the surface. This effect rule makes sense given that the probe's sensitivity increases as the excitation coil's inner diameter decreases. The probe's sensitivity rises linearly with the radius of the excitation coil. Similarly, if the coil has too few turns, the excitation magnetic field signal is too weak to effectively identify defect signals, and if the coil has too many turns, the volume of the coil becomes too high, and the probe's resolution worsens.

Analysis of Detection of Defect and Sorting of Metallic Nano Materials

Modeling metal nanomaterials using finite elements

Surface imperfections and front surface fractures are the primary targets of photoacoustic effect modelling in metal nanomaterials. Optical signals have a hard time detecting surface imperfections since the surface is often polished or coated. Simultaneously, optical signal cannot detect surface fissures that extend to the material's deeper layer. Therefore, surface imperfections and shallow surface fractures are the primary targets of the photoacoustic effect modelling of metal nanoparticles. As the model's dimensions and grid division precision rise, the finite element computation will consume more memory and disc space and take longer to run. The finite element model's steel material properties are used to determine the camera's interior and exterior dimensions, as shown in table 3.

Table 3: Calibration yields both internal and exterior camera parameters.

	Internal factors	External factors
h	457.25	181.46
F	0.01	-0.03
s	3.26	1.16
G	3.23	358.44
K	-0.16	0.016
c	1057.25	334.24

The camera's internal settings are shown in table 3. The camera's calibration involves looking at 12 different factors. The calibration board is a key component of the calibration setup. Both solid board and chessboard designs are frequently used as calibration boards. Depending on the use, you may choose a suitable size. The circular fixed board design on the 50 mm calibration board allows you to choose the calibration. Using a surface array camera, we capture optical data from the rail surface of the dummy body to learn more about the location and size of any surface fractures. This data is used to narrow the laser's scanning region and gather just the optical and acoustic signals near the flaws, reducing the data set size and increasing the detection rate, defects and flaws of various sorts are most common on the surface of metal materials (Figure 2).

If surface flaws can be identified, their origins and evolution may be traced, and the future trajectory of flaws can be predicted.

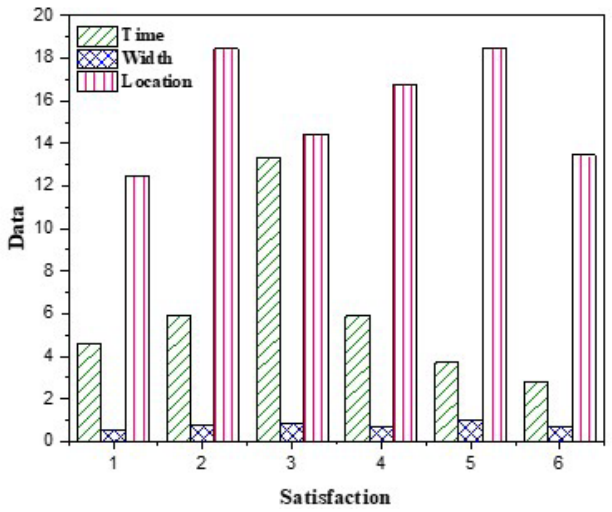

Figure 2: Data from a questionnaire surveying attitudes about English courses in higher education.

Table 4: Metal materials laser energy absorption.

Defect depth	Peak to peak ratio	Peak time	Differential peak	The ratio of time
4	21.466	0.056	9.236	0.951
5	25.664	0.045	10.368	0.926
6	22.135	0.075	13.655	0.669
7	26.688	0.062	13.346	0.883
8	24.455	0.077	14.621	0.845

Table 5: Comprehensive list of characteristics.

Type	A	P	R	Str	C
0	512	298	0.27	26.26	179.35
0	147	97	0.59	11.26	61.46
1	1027	452	0.25	21.26	176.26
1	252	602	0.53	1.36	168.66
2	4452	212	0.67	8.66	71.36
2	212	152	0.78	2.46	766.46

Intensity of laser absorption by metals

Surface imperfections in metals cause significant variations in laser energy absorption because their physical properties, such as density, thermal conductivity, thermal expansion coefficient, and specific heat capacity, differ greatly from those of the metals. Metals with surface flaws have their photoacoustic effect processes simulated. Table 4 displays the results of a comparison between the experimental and simulated data.

Consistent findings between modelling and experiment point to a quadratic function characterising the connection between the electromagnetic signal and the slit defect. Nonetheless, it's worth noting that the results obtained from the finite element simulation model can potentially serve as a substitute for experimental data, as the ratio between the experimental and simulation characteristic signals appears to exhibit a consistent pattern, as indicated in table 4.

The categorization of nano-scale surface defects in metals

To enhance the comprehension of how to classify surface flaws, images of rail surfaces featuring three common defects were utilized. The need for this approach increases, due to the stimulated body employed in the composite experiment being specifically designed to simulate crack faults. Table 5 provides a comprehensive list of characteristics employed to describe these defects, focusing on their geometric properties. These characteristics include dimensions such as, deviation, loft, area circumference ratio, rectangle degree, pulse rate, roundness, and structure. Some defining features of the samples used for training.

Cracks, scale peeling, and fish scale peeling are the three most prevalent forms of surface defects, and as shown in table 5, they were all randomly allocated to different experimental conditions. The results are achieved after the processing method is applied to the training samples. This involves extracting the edges from the images and subsequently computing the feature parameters for each defect. Some distinguishing features of the three sample defect types are discussed in relation to the numbers 0 - 2. Finishing element problems are often tackled using one of two strategies: method of flexibility when internal strength is unknown or method of stiffness when displacement is unknown. Since the stiffness method has more practical applications in actual engineering, it is typically used in the development of finite element software. There are eight stages to developing formulae and solving engineering issues using the finite element method. Typically, the human is responsible for the first and eighth stages (setting and processing), while the computer handles steps two through seven. Figure 3 displays the stress-strain and -displacement connection pertaining to the third iteration of the simulated photoacoustic effect.

The pressure value reflects the vast discrepancy between the impurity part's laser absorption and the non-combustion part's laser absorption because of the compactness of metal materials. This idea suggests using a laser to stimulate the photoacoustic signal of a material's surface at discrete points, with the aim of measuring localised variations in sound pressure. Maximum sound pressure is reflected by light absorption at each place, and the resulting image is faithfully recreated. The light signal may then be used to gauge the breadth of the surface crack and so identify the degradation of contaminants on the material's surface. As can be seen in figure 4, the precision and dependability of the results are enhanced when the photoacoustic signal is enthusiastic at both the borders of the fracture. After doing a qualitative examination of the reflected wave, we compare it to a quantitative computation of the transmitted wave to determine the crack's offset.

This technique was used to measure the depth (within 0.3 mm of accuracy) and the tilt (within 5.4 mm of accuracy). Optical signal detection findings can be used to fine-tune and broaden the photoacoustic signal collection. To manage factors like data size and post-processing time, the yellow box positioned in the center of the figure has been chosen for collecting the photoacoustic signal.

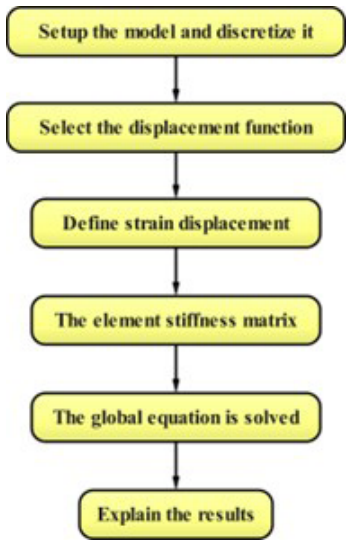

Figure 3: The finite element method: the basic steps.

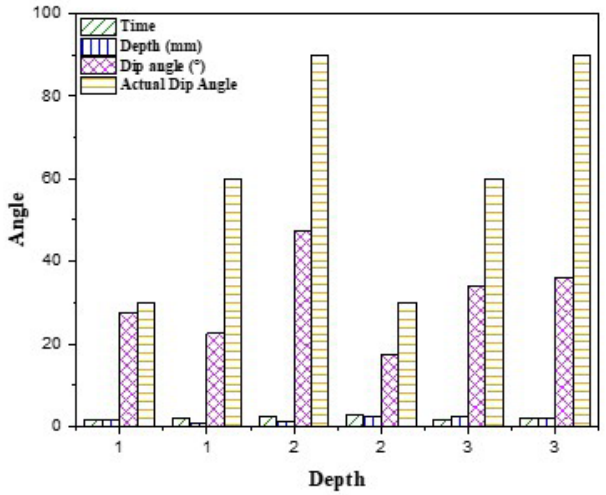

Figure 4: Analyse qualitative of the reflecting wave and computation quantitative of the transmitting wave.

The depth and spectral peak wavelength of cracks, as well as their orientation and location on the surface, are all readily apparent in the reconstructed top 3D pictures. As a result, the photoacoustic signal includes three-dimensional data about forgeries and flaws. Changes in material characteristics due to localised oxidation of the imitator's surface during the experimental stage may also be observed as changes in the photoacoustic pressure at various locations in the 3D picture. Also, this proves the number 333 is correct.

Using an ultrasonic signal and a technique for processing photoacoustic data, a cross-sectional picture of the body model may be generated. Fractures 4, 5, and 6 have a weaker echo signal on the ultrasonic image, and their individual internal extension paths can be seen clearly. One, two, three, seven for the cracks. Since the echo surface is covering the bottom echo signal, isolating it is difficult. This demonstrates the limitations of the ultrasonic approach in detecting shallow faults and makes it inconvenient to quantify the depth of these problems. Since the collected ultrasonic signal exhibits a tracking phenomena, the ultrasonic signal-determined depth of each crack must be given as a range. The ultrasonic signal can only be used to estimate a depth range; from this, it may be deduced that the real depth of a piece crack is somewhere in this limits.

Conclusions

This paper focuses on the analysis and classification of surface defects on metal nanoparticles. It explores various aspects such as the application of DL methods, the development of DL network models, multimode defect detection, and defect simulation. Investigating advanced techniques for characterizing, identifying, and comprehending defect detection in metal nanoparticles using DL is of significant practical significance.

The research entails the analysis of output signals from slit faults at varying depths, utilizing a well-established experimental setup. This setup is commonly employed in contemporary studies related to quantitative defect detection systems. However, it's important to note that the same level of attention and investigation is not typically given to natural cracks encountered in engineering practice.

Smaller than man-made defects, natural fractures have a unique growth process and distinctive signal. Examining quantitative approaches for identifying crack defects, which are often generated by natural sources, this study encourages the extension of quantitative defect detection beyond artificial flaws and into the domain of natural cracks, making a substantial contribution to the subject.

Acknowledgements

None.

Conflict of Interest

None.

References

1. Prasanth IS, Jeevanandam P, Selvaraju P, Sathish K, Ahammad SKH, et al. 2023. Study of friction and wear behavior of graphene-reinforced AA7075 nanocomposites by machine learning. *J Nanomater* 2023: 1-15. https://doi.org/10.1155/2023/5723730
2. Kumar D, Balamurugan A, Suresh KC, Kumar RS, Jayanthi N, et al. 2023. Study of microstructure and wear resistance of AA5052/B4C nanocomposites as a function of volume fraction reinforcement to particle size ratio by ANN. *J Chem* 2023: 1-12. https://doi.org/10.1155/2023/2554098
3. Ieracitano C, Pantó F, Mammone N, Paviglianiti A, Frontera P, et al. 2020. Toward an Automatic Classification of SEM Images of Nanomaterials via a Deep Learning Approach. In Esposito A, Faundez-Zanuy M, Morabito F, Pasero E (eds) Neural Approaches to Dynamics of Signal Exchanges. Smart Innovation, Systems and Technologies, Springer, Singapore, pp 61–72.
4. Xue B, Wu Z. 2022. Defect detection and classification algorithm of metal nanomaterials based on deep learning. *Integr Ferroelectr* 226(1): 277-292. https://doi.org/10.1080/10584587.2022.2065568
5. Girimurugan R, Selvaraju P, Jeevanandam P, Vadivukarassi M, Subhashini S, et al. 2023. Application of deep learning to the prediction of solar irradiance through missing data. *Int J Photoenergy* 2023: 1-17. https://doi.org/10.1155/2023/4717110

6. Ieracitano C, Paviglianiti A, Campolo M, Hussain A, Pasero E, et al. 2020. A novel automatic classification system based on hybrid unsupervised and supervised machine learning for electrospun nanofibers. *IEEE/CAA J Autom Sin* 8(1): 64-76. https://doi.org/10.1109/JAS.2020.1003387
7. Liu H. 2022. Clothing nanometer antimite and antibacterial based on deep learning technology. *J Nanomater* 2022: 1-13. https://doi.org/10.1155/2022/4916197
8. Riveiro B, Solla M. 2016. Non-Destructive Techniques for the Evaluation of Structures and Infrastructure. CRC Press, Boca Raton, FL, USA.
9. Kaur K, Mulaveesala R, Mishra P. 2021. Constrained autoencoder-based pulse compressed thermal wave imaging for sub-surface defect detection. *IEEE Sens J* 22(18): 17335-17442. https://doi.org/10.1109/JSEN.2021.3056394
10. Pyle RJ, Hughes RR, Ali AA, Wilcox PD. 2022. Uncertainty quantification for deep learning in ultrasonic crack characterization. *IEEE Trans Ultrason Ferroelectr Freq Control* 69(7): 2339-2351. https://doi.org/10.1109/TUFFC.2022.3176926
11. Cheng X, Chen P, Wu Z, Cech M, Ying Z, et al. 2023. Automatic detection of CFRP subsurface defects via thermal signals in long pulse and lock-in thermography. *IEEE Trans Instrum Meas* 72. https://doi.org/10.1109/TIM.2023.3277996
12. Wang W. 2023. Surface defects detection in metal materials repaired by laser surfacing of seal welds. *J Mea Eng* 11(3): 343-357. https://doi.org/10.21595/jme.2023.23316
13. Wang R, Cheung CF, Wang C. 2023. Unsupervised defect segmentation in selective laser melting. *IEEE Trans Instrum Meas* 72. https://doi.org/10.1109/TIM.2023.3291002
14. Kalimullah NM, Shelke A, Habib A. 2023. A deep learning approach for anomaly identification in PZT sensors using point contact method. *Smart Mater Struct* 32(9): 095027. https://doi.org/10.1088/1361-665X/acee37
15. Satishkumar P, Mahesh G, Meenakshi R, Vijayan SN. 2021. Tribological characteristics of powder metallurgy processed Cu-WC/SiC metal matrix composites. *Mater Today Proc* 37: 459-465. https://doi.org/10.1016/j.matpr.2020.05.449
16. Elsheikh AH, Shanmugan S, Muthuramalingam T, Thakur AK, Essa FA, et al. 2022. A comprehensive review on residual stresses in turning. *Adv Manuf* 1-26. https://doi.org/10.1007/s40436-021-00371-0
17. Satyanarayana G, Narayana KL, Rao BN. 2021. Incorporation of Taguchi approach with CFD simulations on laser welding of spacer grid fuel rod assembly. *Mater Sci Eng* 269: 115182. https://doi.org/10.1016/j.mseb.2021.115182
18. Satishkumar P, Rakesh AI, Meenakshi R, Murthi CS. 2021. Characterization, mechanical and wear properties of Al6061/Sicp/fly ashp composites by stir casting technique. *Mater Today Proc* 37: 2687-2694. https://doi.org/10.1016/j.matpr.2020.08.530
19. Satishkumar P, Krishnan GG, Seenivasan S, Rajarathnam P. 2023. A study on tribological evaluation of hybrid aluminium metal matrix for thermal application. *Mater Today Proc* 81: 1097-1104. https://doi.org/10.1016/j.matpr.2021.04.389
20. Dharmaiah G, Sridhar W, Balamurugan KS, Chandra Kala K. 2022. Hall and ion slip impact on magneto-titanium alloy nanoliquid with diffusion thermo and radiation absorption. *Int J Ambient Energy* 43(1): 3507-3517. https://doi.org/10.1080/01430750.2020.1831597
21. Abushanab WS, Moustafa EB, Harish M, Shanmugan S, Elsheikh AH. 2022. Experimental investigation on surface characteristics of Ti6Al4V alloy during abrasive water jet machining process. *Alex Eng J* 61(10): 7529-7539. https://doi.org/10.1016/j.aej.2022.01.004
22. Xian Y, Yu Y, Lian Y, Fan J, Wang Z. 2023. An EA-based pruning on improved YOLOv3 for rapid copper elbow surface defect detection. *Eng Appl Artif Intell* 123: 106412. https://doi.org/10.1016/j.engappai.2023.106412
23. Chen P, Yang J, Wang R, Xiao B, Liu Q, Sun B, et al. 2022. Graphene oxide enhanced the endocrine disrupting effects of bisphenol A in adult male zebrafish: integrated deep learning and metabolomics studies. *Sci Total Environ* 809: 151103. https://doi.org/10.1016/j.scitotenv.2021.151103